EURASIAN PHYSICAL TECHNICAL JOURNAL

2026, Volume 23, No.2 (56)

https://doi.org/10.31489/2026N2/35-46

Received: 12/015/2025 Revised: 29/04/2026 Accepted: 26/06/2026 Published online: 30/06/2026

Original Research Article

UDC 533.0.01; 621.548.5

ANALYSIS OF AERODYNAMICS OF AN ASYMMETRIC DARRIEUS WIND TURBINE WITH THREE-BLADES

Manatbayev R.[1], Kalassov N.[1], Seydulla Zh.[1], Isataev M.[1], Baizhuma Zh.[1], Kuykabayeva A.[1], Rasul K.[1]*

Al-Farabi Kazakh National University, Almaty, Kazakhstan
*Corresponding author: kozhash@list.ru

Abstract. *This paper presents a comprehensive numerical investigation of the aerodynamic performance of a three-bladed vertical-axis Darrieus wind turbine equipped with asymmetric airfoil blades, with the primary aim of evaluating the influence of blade geometry on torque generation and overall aerodynamic efficiency. The study focuses on a detailed analysis of rotor flow behavior, including the spatial distributions of velocity and pressure fields, the formation and evolution of flow separation zones, and the development of a turbulent wake structure downstream of the rotor over a wide range of operating conditions. Numerical simulations were carried out using the Reynolds-Averaged Navier–Stokes equations coupled with the k–ω SST turbulence model, which provides reliable prediction of near-wall flow behavior, adverse pressure gradients, and unsteady aerodynamic effects typical for vertical-axis wind turbines. The obtained results demonstrate that the asymmetric blade profiles interact more effectively with the incoming airflow at moderate tip speed ratio values, leading to improved torque characteristics and a noticeable reduction in negative torque regions. In particular, the maximum average torque coefficient was observed at tip speed ratio values close to 2.5, where the aerodynamic performance of the rotor reached its optimum due to balanced lift and drag forces acting on the blades. At higher tip speed ratio values, despite the stabilization of the flow structure and reduction of large-scale vortical formations, a decrease in aerodynamic efficiency was identified, and the findings of this study provide a scientific basis for optimizing blade geometry and selecting efficient operating regimes in the design of Darrieus-type vertical-axis wind turbines with asymmetric airfoils.*

Keywords: Vertical-axis wind turbine; Darrieus rotor; asymmetric airfoil; aerodynamic performance; torque coefficient; tip speed ratio.

1. Introduction

Increasing global warming and growing concerns about environmental degradation are prompting many countries to reduce their dependence on fossil fuels and transition to clean energy sources. Wind energy holds a special place among renewable energy sources due to its abundant reserves, inexhaustible nature, and low environmental impact. Modern scientific research in this field demonstrates that wind energy has high potential to complement or replace traditional energy sources. Wind turbines are the primary technical devices for the efficient use of wind energy. A wind turbine is a complex engineering system designed to convert the kinetic energy of atmospheric airflow into mechanical energy and then into electrical energy [1]. Its operating principle is based on the coordinated control of aerodynamic forces and energy conversion processes, which determines the overall efficiency and energy productivity of the system. Depending on their axis of rotation, wind turbines can be divided into horizontal-axis wind turbines (HAWT) and vertical-axis wind turbines (VAWT) [2]. Horizontal-axis wind turbines (HAWT) are currently the most widely used wind turbines in large

wind farms due to their high efficiency [3]. However, vertical-axis wind turbines (VAWT) have distinct advantages. They are particularly suitable for use in turbulent or urban environments. Vertical-axis wind turbines (VAWTs) have not yet been fully studied [4]. This is mainly due to the fact that the aerodynamic characteristics of vertical-axis wind turbines are more complex than those of horizontal-axis wind turbines. However, VAWT offer unique advantages, including ease of design and maintenance [5], the ability to operate in any wind direction without the need for expensive turning mechanisms [6], low noise levels, and suitability for installation in urban areas [7, 8]. Recent recognition of the structural and aerodynamic advantages of vertical-axis wind turbines has led to a revival of this trend and the need for extensive scientific research [9-11]. One of the key elements determining the efficiency of the Darie wind turbine is the blade profile. Symmetrical and asymmetrical profiles are used in design practice, each with its own advantages and disadvantages. Symmetrical blades have identical upper and lower surfaces, while asymmetrical blades have different upper and lower surfaces. Asymmetrical blades are more efficient than symmetrical ones in areas with low and variable wind speeds due to their high starting torque and self-starting capability. Asymmetrical blades have been extensively studied in recent years to improve the aerodynamic performance of vertical-axis wind turbines and offer several significant advantages over symmetrical profiles. Therefore, another effective solution for increasing the power of vertical-rotor wind turbines is the development of specialized airfoils for such turbines, as they can significantly impact wind energy efficiency and the flow field around the blade [12]. Asymmetric airfoils, characterized by a curved shape, improve the aerodynamic performance of wind turbines under various conditions. For example, [13] showed that by optimizing the angle of asymmetric blades, performance at low wind speeds can be significantly improved.

The growing interest in asymmetric blades is explained by their ability to control complex flow processes. Asymmetric geometry balances aerodynamic loads during the positive and negative half-periods of the rotor, preventing flow interruption or stall. At the same time, such modifications can improve the maximum power factor (Cp) of the rotor not only at medium speeds but also in low- tip speed ratio (TSR) regimes. For example, [14–15] demonstrated that an asymmetric blade profile not only improves self-starting performance compared to a symmetric blade profile but also increases (Cp) by up to 26.83%. This makes vertical-axis wind turbines suitable for regions with low wind speeds, thereby expanding their application range.

Asymmetric and modified blades for vertical-axis Darrieus wind turbines have been shown to improve aerodynamic efficiency in low-TSR regimes [16–19]. Experimental and numerical analyses confirm that blade geometry directly influences the formation of pressure, velocity, and torque fields. These results support the relevance of in-depth numerical studies of asymmetric blades.

Thus, the literature review demonstrates that the use of asymmetric blades can significantly improve the aerodynamic performance of vertical-axis Darrieus wind turbines.

2. Methodology

2.1 Model geometry

Figure 1 shows the geometric model of an asymmetric three-bladed Darrieus wind turbine. In this study, the aerodynamic characteristics of an asymmetric three-bladed Darrieus vertical-axis wind turbine were analyzed using numerical simulation methods. The primary objective of the study was to evaluate the impact of asymmetric blade geometry on rotor performance and determine the aerodynamic efficiency under various operating conditions.

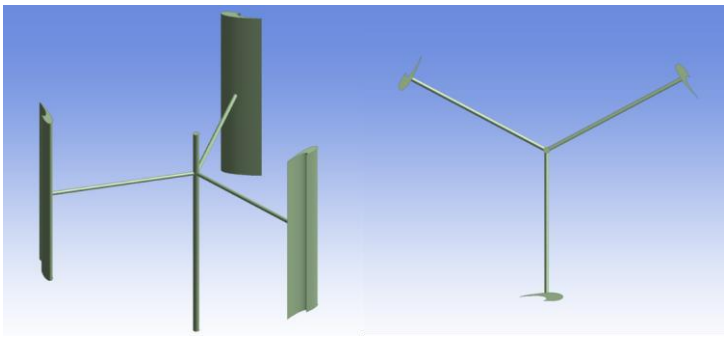

Fig.1. Asymmetric three-bladed Darrieus wind turbine.

The object of the study was an asymmetric configuration of a three-bladed Darrieus rotor. The blade shape was achieved by modifying the aerodynamic profiles to improve the interaction of the rotor with the wind flow at different phases. Table 1 shows the geometric parameters of the vertical-axis Darrieus turbine; this data is taken from the article [20]. As shown in Figure 2, a rectangle and a cylinder were chosen as the computational domain. We consider the rectangle as a stationary domain, and the cylinder as a moving domain. This approach allowed us to accurately represent the flow around the rotor and the interaction of the airflow with its blades. Table 2 shows the geometric parameters of the computational domain, taken from [20].

Table 1. Geometrical parameters of the vertical-axis Darrieus turbine.

Parameter	Mean
Aerodynamic profile	NACA 0021
Number of blades (N)	3
Chord length (C)	0,04 m
Rotor diameter (D)	3 m
Relative density of the turbine (σ)	0,3

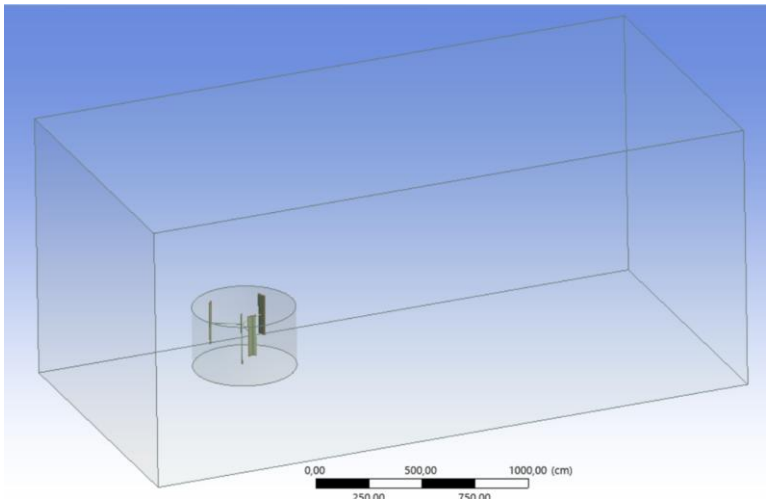

Fig.2. Computational domain of an asymmetric three-bladed Darrieus wind turbine.

Table 2. Geometric parameters of the computational domain for modeling the aerodynamics of an asymmetric three-bladed Darrieus wind turbine.

Parameter	Mean
Rotor diameter	D
Moving domain diameter	1,5D
Distance from the rotor center to the left border	20D
Distance from the rotor center to the right border	40D
Distance from the rotor center to the upper and lower boundaries	10D

One way to improve the Darrieus rotor is to introduce controlled geometric asymmetry into the blade configuration. Geometric modification improves the aerodynamic interaction of the blade with the airflow, expands the range of operating angles of attack, and increases torque stability. This study proposes the design of a three-bladed asymmetric Darrieus wind turbine, where the asymmetry is formed based on a combination of NACA0021 airfoils [21–24]. By trimming the main airfoil to a smaller airfoil, we obtain a modified NACA0021 blade, shown in Fig3.

This approach allows for the redistribution of loads along the arc of rotation, altering the blade's thickness, surface area, and local aerodynamic curvature. This improves the lift-to-drag ratio, potentially increasing the rotor's power factor. Furthermore, the proposed geometric design reduces vibration loads and torque fluctuations, a crucial factor for low-power vertical-axis wind turbines.

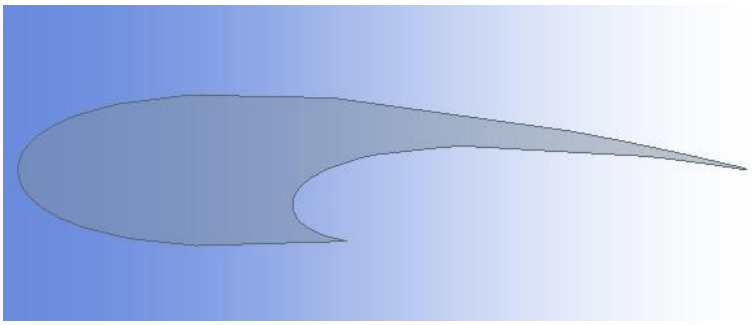

Fig.3. Asymmetrical blade NACA 0021

To provide a quantitative description of the blade geometry and to improve the reproducibility of the numerical model, the coordinate data of the NACA 0021 profile were analyzed. The chord length in the coordinate file is equal to 400 coordinate units and was scaled to the chord length used in the numerical model, C = 0.04 m. The maximum profile thickness obtained from the coordinates is tmax/C = 0.2100, which corresponds to the NACA 0021 airfoil. The maximum thickness is located at xt/C = 0.3014. The main geometrical parameters extracted from the coordinate data are presented in Table 3.

Table 3. Geometrical parameters of the blade profile based on the coordinate data.

Parameter	**Symbol**	**Value**
Initial aerodynamic profile	—	NACA 0021
Chord length	C	0.04 m
Chord length in coordinate data	Ccoord	400
Maximum upper-surface ordinate	ymax/C	0.1050
Maximum lower-surface ordinate	ymin/C	−0.1050
Maximum profile thickness	tmax/C	0.2100
Maximum profile thickness	tmax	0.0084 m
Position of maximum thickness	xt/C	0.3014
Leading-edge coordinate	x/C; y/C	0; 0
Trailing-edge coordinate	x/C; y/C	1; 0
Trailing-edge thickness	δTE/C	0
Number of coordinate points	Np	201

2.2 Basic Equations

Dimensionless aerodynamic parameters such as the power coefficient (Cp), torque coefficient (Cm), lift coefficient (Cl), and drag coefficient (Cd) are used to quantify the aerodynamic performance of a wind turbine. These coefficients allow one to determine the turbine's energy efficiency and compare the obtained calculation results. The actual power (P) extracted by the turbine from the flow is determined by the ratio of its theoretical maximum power (P_a), and the power coefficient is given by the following expression:

$$C_P = \frac{P}{\frac{1}{2}\rho A V^3} \quad (1)$$

where ρ – air density (kg/m³), A – rotor projection area (m²), and V – wind speed at the inlet (m/s).

The power generated by a turbine is determined by the product of torque (T) and angular velocity (ω):

$$P = T \cdot \omega \quad (2)$$

Using this relationship, the power factor can be expressed in terms of torque characteristics:

$$C_P = \frac{T \cdot \omega}{\frac{1}{2}\rho A V^3} \quad (3)$$

The torque coefficient (Cm) is determined by the following formula:

$$C_M = \frac{T}{\frac{1}{2}\rho A R V^3} \quad (4)$$

where R – rotor radius (m).

The relationship between Cp and Cm is defined as follows:

$$C_P = C_M \cdot \lambda \quad (5)$$

where $\lambda = \frac{\omega R}{V}$ – blade TSR.

The physical model of flow near a blade surface is based on the laws of conservation of mass, momentum, and energy. For incompressible and isothermal airflow, these processes are described by the Navier-Stokes equations:

$$\nabla \cdot u = 0 \quad (6)$$

$$\frac{\partial u}{\partial t} + (u \cdot \nabla)u = -\frac{1}{\rho}\nabla p + \nu \nabla^2 u + f \quad (7)$$

where u – flow velocity vector, p – pressure, ρ – air density, ν – kinematic viscosity, f – mass forces. Here, f is the body force term. In this study, body forces were neglected due to their insignificant influence on the considered incompressible and isothermal airflow; therefore, f = 0 was used in the numerical simulations.

Because direct numerical modeling (DNS) is computationally expensive for high-Reynolds number flows, Reynolds-averaged Navier-Stokes (RANS) equations are used in engineering calculations. Averaging leads to turbulent Reynolds stresses, so a turbulence model must be introduced to describe the system. The averaged continuity equation is:

$$\frac{\partial \overline{u_i}}{\partial x_i} = 0 \quad (8)$$

The average momentum equation is:

$$\frac{\partial \overline{u_i}}{\partial t} + \overline{u_j}\frac{\partial \overline{u_j}}{\partial x_j} = -\frac{1}{\rho}\frac{\partial \overline{p}}{\partial x_i} + \nu \frac{\partial^2 \overline{u_i}}{\partial x_j^2} - \frac{\partial \tau_{ij}}{\partial x_j} \quad (9)$$

where $\overline{u_i}$ – average flow rate, $\tau_{ij} = \overline{u_i' u_j'}$ – Reynolds tensor of turbulent stresses.

To fully capture the system, the k-ω SST turbulence model, widely used in engineering aerodynamics, was chosen. This model allows for synergy with the k-ε model in the free-flow zone while maintaining accuracy in high-gradient regions. The model consists of two main auxiliary equations: the turbulent kinetic energy (k) and the specific dissipation rate (ω):

$$\frac{\partial(\rho k)}{\partial t} + \frac{\partial(\rho u_j k)}{\partial x_j} = P_k - \beta^* \rho \omega k + \frac{\partial}{\partial x_j}\left[(\mu + \sigma_k \mu_t)\frac{\partial k}{\partial x_j}\right] \quad (10)$$

$$\frac{\partial(\rho \omega)}{\partial t} + \frac{\partial(\rho u_j \omega)}{\partial x_j} = \gamma \frac{\omega}{k} P_k - \beta \rho \omega^2 + \frac{\partial}{\partial x_j}\left[(\mu + \sigma_\omega \mu_t)\frac{\partial \omega}{\partial x_j}\right] + 2(1 - F_1)\rho \sigma_{\omega 2}\frac{1}{\omega}\frac{\partial k}{\partial x_j}\frac{\partial \omega}{\partial x_j} \quad (11)$$

where ρ – density, k – turbulent kinetic energy, P_k – a source of turbulent energy caused by a change in velocity, β^*, γ, β – empirical constants, ω – specific dissipation rate, μ – dynamic viscosity, μ – turbulent viscosity, σ_k – diffusion coefficient for k.

The system of governing equations (6)–(11) was solved using the finite volume method. A transient pressure-based solver was applied to describe the unsteady aerodynamic interaction between the rotating blades and the airflow. Pressure–velocity coupling was performed using the SIMPLE algorithm. The pressure equation was discretized using a second-order scheme, while the convective terms in the momentum and turbulence equations were approximated by a second-order upwind scheme. The transient terms were discretized using a second-order implicit formulation. The gradients were calculated using the least-squares cell-based method. The convergence criterion for the residuals of the governing equations was set to 10^{-5}, and

the torque coefficient was additionally monitored until a periodic solution was obtained over several complete rotor revolutions.

The computational domain consisted of an inner rotating cylindrical region and an outer stationary rectangular region. The rotating region contained the three-bladed rotor, and its angular velocity was prescribed according to the selected TSR value. The outer region remained stationary and represented the far-field flow with specified inlet, outlet, and side boundary conditions. The RANS equations with the k–ω SST turbulence model were solved in both regions using the finite volume method. The interaction between the rotating and stationary domains was implemented through a sliding mesh interface, where pressure, velocity, and turbulence quantities were exchanged at each time step.

2.3 Mesh generation

In this study, a multi-layer hybrid mesh was used to accurately calculate the aerodynamic characteristics of a wind turbine. The mesh structure is designed to accurately represent the boundary layer near the blade, vortex shedding regions, and complex flow fields around the rotor. The images below illustrate the mesh features in various regions.

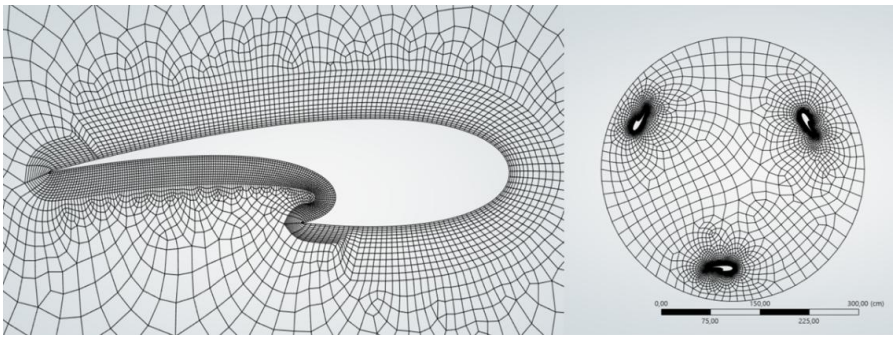

Fig.4. Mesh near the NACA0021 asymmetric blade

The mesh shown in Figure 4 is a multi-block hybrid structure designed to accurately discretize the flow region near a blade airfoil. In the region close to the blade surface, prismatic elements with 15–25 layers are used to accurately describe the boundary layer, ensuring the condition $y^+ \approx 1–5$, while the mesh is significantly denser to correctly account for sharp changes in pressure gradients at the leading and trailing edges. As the distance from the blade increases, the element sizes gradually increase in accordance with geometric patterns, improving the computational efficiency of the entire domain. While the structured regions of the mesh accurately capture the complex geometry of the airfoil, the free-form elements in the outer regions do not disrupt the natural flow distribution. Overall, this mesh enables highly accurate computation of turbulent flow–especially vortex structures at the blade tip and separation zones at the rear.

The mesh configuration in Figure 5 is designed to discretize the entire flow domain of a vertical-axis Darrieus wind turbine and accurately model aerodynamic phenomena around a rotor with complex geometry. The three-dimensional mesh of the rectangular computational domain (left figure) is formed using mesh densification near the rotor to accurately determine vortex structures, flow separation, and low-pressure zones in the rotor region.

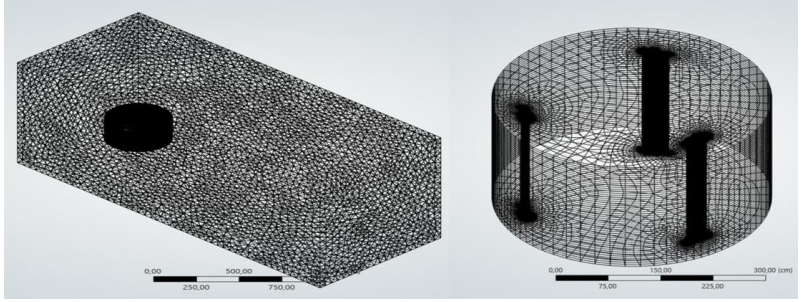

Fig.5. Grid of computational domains for an asymmetric three-bladed Darrieus wind turbine.

In distant regions, element sizes gradually increase, reducing the overall computational load. In regions close to the cylindrical rotor body located in the center, triangular-tetrahedral meshes ensure a natural flow distribution along the complex geometry. The mesh of the three-bladed rotor, located within the cylindrical region shown in the figure on the right, is based on a multi-block structured system. To accurately model the boundary layer near each blade, concentric layers are formed in the radial direction, and the mesh is particularly fine in the high-gradient regions near the blade tips. The cylindrical outer boundary ensures constant flow conditions at the outlet and inlet, while maintaining the geometric consistency of the mesh. Overall, the mesh quality enables highly accurate calculations of flow variations.

2.4 Grid and time-step independence analysis

To ensure the stability and reliability of the obtained numerical results, a convergence analysis of the numerical solution was carried out during the CFD simulations. During the calculations, the residuals of the governing equations were monitored, and the stabilization of the main aerodynamic parameters, including the torque coefficient (Cm), was analyzed over several complete rotor revolutions. In addition, a grid independence study was performed to evaluate the influence of mesh resolution on the calculated aerodynamic characteristics.

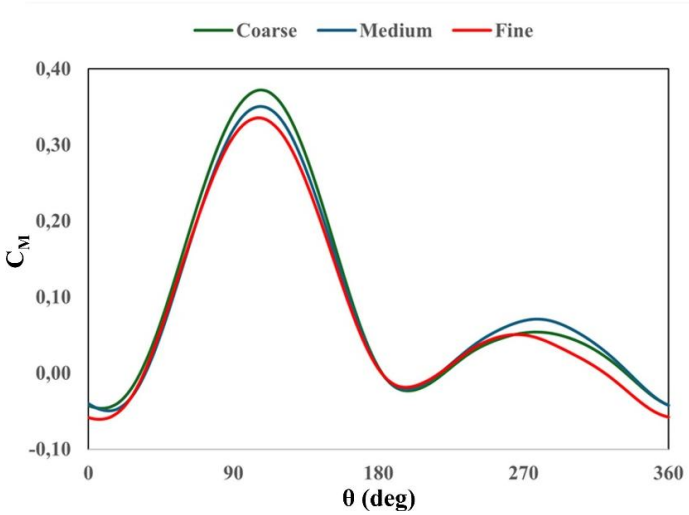

Fig.6. Mesh sensitivity analysis.

Three mesh levels, namely coarse, medium, and fine, were considered, as shown in Table 4. The comparison was performed for the representative operating condition TSR = 2.5, where the rotor demonstrates the highest positive torque coefficient and the maximum average useful torque. The average torque coefficient and power coefficient were selected as the main convergence criteria.

Table 4. Grid convergence analysis

Mesh type	Number of elements	Type of elements	First layer thickness	y^+
Coarse	486,325	Predominantly triangular elements	5×10^{-4} m	6.8
Medium	1,204,786	Hybrid mesh (quadrilateral + triangular elements)	10^{-5} m	0.85
Fine	2,148,532	Fine hybrid mesh with quadrilateral refinement	10^{-6} m	0.12

3. Results and discussion

As the rotor rotates, the blade's angle of attack constantly changes, which in turn directly affects the pressure distribution and the formation of flow lines on the blade surface. While pressure contours indicate the location of high and low pressure regions, flow lines visually describe the overall flow dynamics. The configuration and location of these regions constantly change as the rotor rotates, so it is important to analyze changes in the pressure field and flow structure at different rotation angles.

In this regard, the study comprehensively examined pressure changes and flow structure reorganization at various rotor azimuthal positions. This analysis allows us to determine the characteristics of airflow-blade interactions and assess the impact of the angle of attack on turbine aerodynamic performance. The results obtained provide the basis for a deeper understanding of time-dependent flow behavior during rotor operation and for analyzing the effectiveness of blade geometry.

3.1 Pressure contour

Figure 7 shows the numerical results of the pressure distribution for a three-bladed Darrieus rotor with a modified asymmetric profile. There are the static pressure contours for various TSR values for a three-blade Darrieus rotor with an asymmetric profile. At low TSR values (1.5–2.0), high-pressure zones are clearly visible on the leading edge of the blades, while low-pressure zones are visible on the trailing edge, indicating a high aerodynamic load on the rotor. As the TSR value increases (2.5–3.0), the pressure field somewhat equalizes, and the distribution of high- and low-pressure zones stabilizes. At high TSR values (3.5–5.0), the pressure gradient decreases, and a uniform flow distribution around the rotor is observed, indicating stabilization of aerodynamic interactions and a stable operating mode.

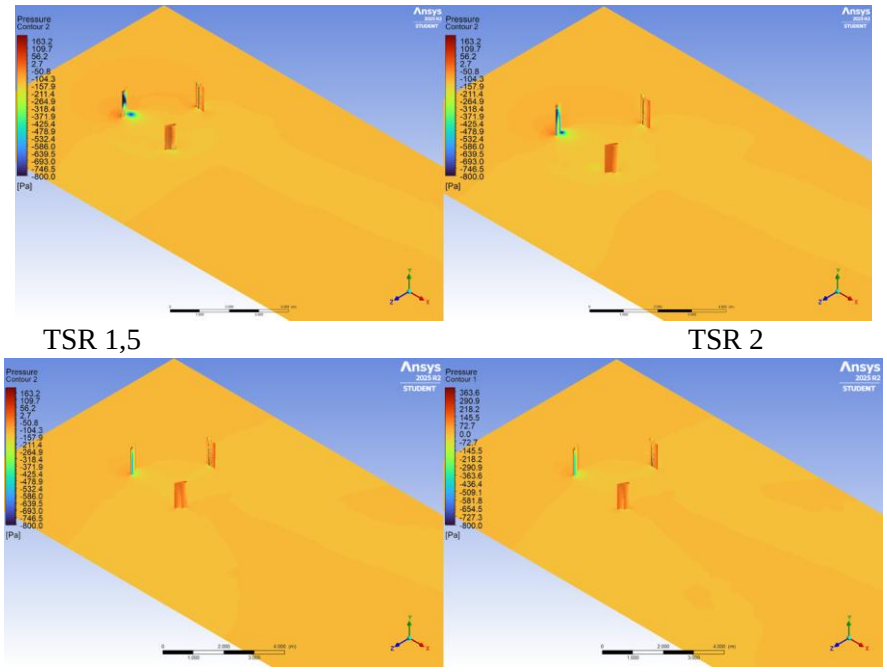

Fig.7. Contours of static pressure around an asymmetric 3-blade Darrieus rotor at different values of TSR.

3.2 Turbulent wake contour

Figure 8 shows the turbulent wake contours for a three-blade Darrieus rotor with an asymmetric airfoil at different TSR values. At low TSR values (1.5–2.0), distinct and irregular turbulent structures form behind the rotor, and a high level of vorticity is observed. As the TSR value increases (2.5–3.0), the turbulent wake lengthens, its structure becomes somewhat more regular, and energy losses are gradually distributed along the flow. At high TSR values (3.5–5.0), the turbulent wake intensity decreases, and the vortex amplitude decreases, indicating flow stabilization and improved rotor aerodynamic performance.

3.3 Change in torque coefficient at different TSR values per one complete revolution

Figure 9 shows a comparative dependence of the torque coefficient (Cm) on the azimuth angle (Θ) for a three-bladed Darrieus rotor with an asymmetric profile at TSR = 1.5–5.0. These results clearly illustrate the nature of the change in aerodynamic load and the differences in efficiency in different rotor operating modes.

At low and medium TSR values (TSR = 1.5–3.0), the Cm amplitude is significantly higher, and oscillations are clearly visible. Especially at TSR = 2.5, the highest positive torque coefficient values are recorded, and the influence of negative torque zones is weak. In this mode, the blade angle of attack is in the aerodynamically favorable range, and lift is generated efficiently. As a result, the average useful torque obtained from the rotor is maximum, characterizing the TSR = 2.5 mode as the most efficient operating zone.

Although positive Cm values predominate at TSR = 1.5 and TSR = 2.0, the presence of regions with oscillation amplitude and negative torque indicates a more frequent occurrence of flow separation. This situation reduces rotor stability and limits overall energy efficiency. In the high TSR region (TSR = 3.5–5.0), the Cm curves flatten out, and the oscillation amplitude decreases significantly.

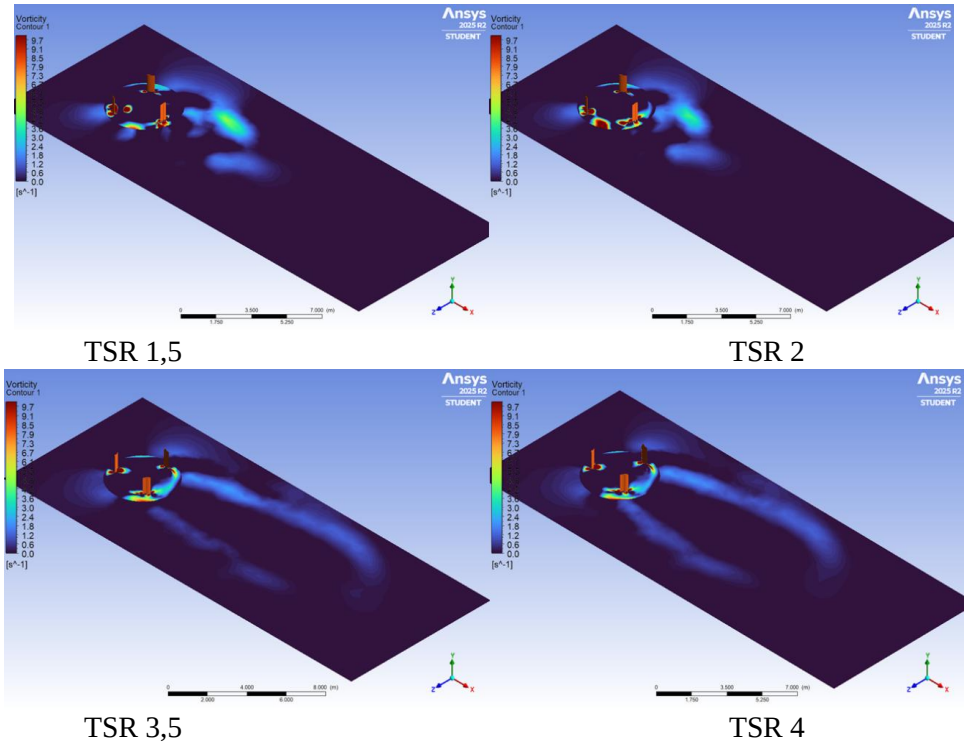

Fig.8. Turbulent wake contours generated by an asymmetric 3-blade Darrieus rotor at different TSR values.

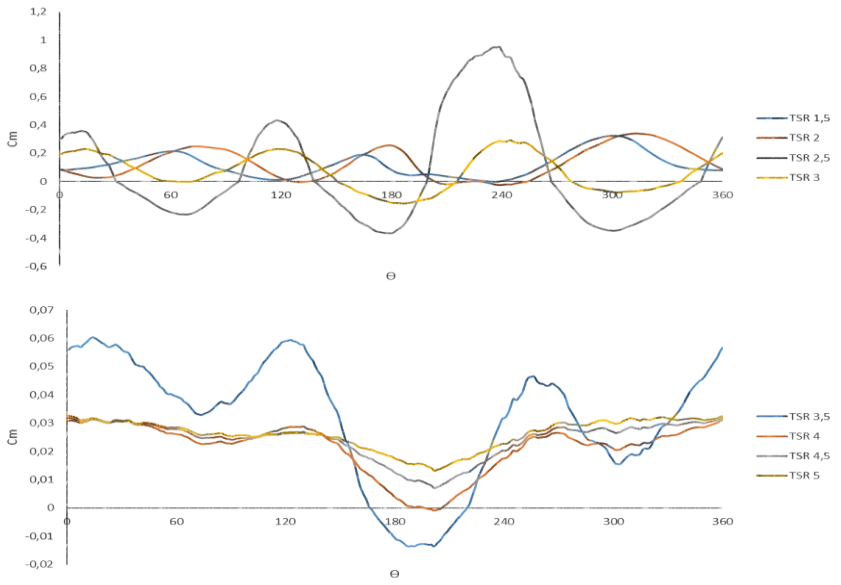

Fig.9. Variation of the torque coefficient Cm for asymmetric blades at full rotation at different values of TSR.

However, this stability is accompanied by a decrease in the average torque coefficient. At TSR = 3.5, a negative torque is observed in a certain azimuthal region (approximately 170–210°), indicating increased inertial and aerodynamic losses. In TSR = 4.0–5.0 regimes, although the negative torque regions weaken, the positive torque also remains low, which is explained by the inability of the blades to fully effectively extract energy from the flow.

A general comparative analysis revealed that the most favorable combination of torque coefficient and maximum average value is achieved in the TSR range of 2.5. This finding confirms the aerodynamic advantage of asymmetric blades in medium TSR modes and the limited optimal operating range for Darrieus-type vertical-axis wind turbines.

3.4 Power factor versus TSR

Figure 10 shows a comparison of the power factor Cp as a function of TSR for an asymmetric 3-blade wind turbine, where the experimental values are taken from the literature [25]. For the asymmetric blade (blue line), the power factor increases as TSR increases from 1.5 to the range of 2.0–2.2, reaching its maximum value around Cp ≈ 0.24–0.25. This range is the most efficient operating mode of the turbine. As TSR further increases (after 2.5), Cp gradually decreases. At TSR ≈ 4–5, the power factor decreases significantly, indicating an increase in aerodynamic losses. This phenomenon is explained by the flow disturbance in the blade, increased turbulence, and inefficiency of the rotation mode.

According to experimental data (red line), Cp starts at low values and steadily increases with increasing TSR. The maximum power factor is observed in the range of TSR ≈ 3.2–3.5, reaching Cp ≈ 0.28–0.29. This value indicates that the efficient operating mode is achieved at increasingly higher TSR values than the calculated maximum obtained for the asymmetric blade.

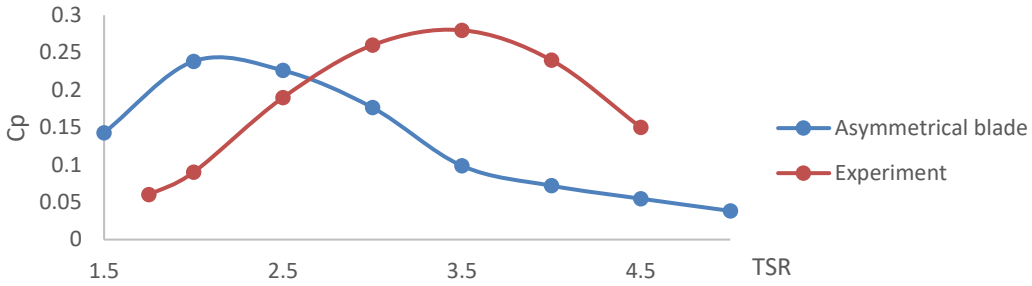

Fig.10. Power factor Cp versus TSR for an asymmetric 3-blade wind turbine.

It should be noted that the comparison between the experimental and numerical results is qualitative rather than a direct one-to-one validation, since the experimental data correspond to a turbine with a symmetric blade profile, whereas the present CFD results were obtained for a modified asymmetric blade. The discrepancy in the maximum Cp value and optimal TSR can be explained by differences in blade geometry, rotor scale, Reynolds number, three-dimensional flow effects, end losses, support elements, mechanical losses, and idealized CFD boundary conditions. Nevertheless, both curves show the same general trend: Cp increases with TSR up to an optimal range and then decreases due to aerodynamic losses, wake development, and flow separation. Therefore, the comparison confirms the physical consistency of the numerical results, while further experimental validation of the proposed asymmetric blade geometry is required.

4. Conclusion

This study, using numerical simulations and experimental data, conducted a comprehensive analysis of the aerodynamic and energy characteristics of a vertical-axis wind turbine with asymmetric blades. The results showed that the power factor (Cp) depends on the total speed ratio (TSR) and that blade geometry plays a decisive role in determining turbine efficiency.

An analysis of the power factor versus TSR curves showed that the highest efficiency of the asymmetric blade is observed at low and medium TSR values (approximately TSR ≈ 2.5). At this point, Cp reaches its maximum value, demonstrating the turbine's ability to efficiently generate power even at low rotational speeds. With further increases in TSR, Cp gradually decreases, which is associated with increased aerodynamic losses, flow disturbance zones, and turbulence levels at high rotational speeds.

According to experimental data, the maximum power factor is observed at higher TSR values (TSR ≈ 3–3.5), and the maximum Cp value is higher than that of the asymmetric computational model. This indicates the complexity of inertial effects, three-dimensional flow structures, and blade-flow interactions under real-world conditions. At the same time, this difference highlights the need to refine the computational model and the importance of adapting the turbine operating mode to real-world conditions.

An analysis of the flow velocity and pressure contours showed that the load is uniformly distributed across the asymmetric blade, and in the effective TSR region, high-velocity flows continuously form on the blade surface. In inefficient modes (at high TSR), the contours show an increase in turbulent zones, an increase in vortices, and a decrease in the pressure difference, which directly contributes to a reduction in the power factor. Overall, the obtained results demonstrate the effectiveness of a vertical wind turbine with asymmetric

blades in areas with low wind speeds and low relative drag coefficients. This design makes it promising for use in areas with light to moderate wind conditions. The study's findings can serve as a basis for optimizing wind turbine blade geometry, increasing their energy efficiency, and further improving their aerodynamic performance.

Conflict of interest statement

The authors declare that they have no conflict of interest in relation to this research, whether financial, personal, authorship or otherwise, that could affect the research and its results presented in this paper.

CRediT author statement

Manatbayev R.: data curation, validation; Kalasov N.: investigation, funding acquisition; Seydulla Z.: writing – review & editing; Isataev M.: visualization & methodology; Baizhuma Z.: supervision, conceptualization; Kuykabayeva A.: resources, formal analysis; Kozhash R.: writing original draft, modeling. The final manuscript was read and approved by all authors.

Statement on the use of Artificial Intelligence.

The authors declare that no artificial intelligence tools were used to generate scientific content, results, or conclusions of this article.

Data Availability Statement

The data are available upon reasonable request from the authors.

Funding

This research has been funded by the Science Committee of the Ministry of Science and Higher Education of the Republic of Kazakhstan (Grant No. BR28713563, «Hybrid wind-solar power system with intelligent control to improve energy efficiency in different climate conditions»).

References

1 Li, C., Zhu, S., Xu, Y.L., Xiao, Y. (2013). 2.5D large eddy simulation of vertical axis wind turbine in consideration of high angle of attack flow, Renew. *Energy*, 51, 317–330. https://doi.org/10.1016/j.renene.2012.09.011

2 Shukla, V., Kaviti, A. (2017). Performance evaluation of profile modifications on straight-bladed vertical axis wind turbine by energy and Spalart Allmaras models. *Energy*, 126, 766-95. https://doi.org/10.1016/j.energy.2017.03.071

3 Murata, J., Endo, M., Maeda, T. (2016). Experimental and numerical investigation of the effect of turbulent inflow on a Horizontal Axis Wind Turbine (part I: power performance). *Energy*, 113, 713–722. https://doi.org/10.1016/j.energy.2016.06.138

4 Hameed, M., Afaq, S.K. (2013). Design and analysis of a straight bladed vertical axis wind turbine blade using analytical and numerical techniques. *Ocean Eng*, 57, 248–55. https://doi.org/10.1016/j.oceaneng.2012.09.007

5 Liu, J., Lin, H., Zhang, J. (2019). Review on the technical perspectives and commercial viability of vertical axis wind turbines. *Ocean Eng.*, 15, 608–626. https://doi.org/10.1016/j.oceaneng.2019.04.086

6 Islam, M., Ting, D.K., Fartaj, A. (2008). Aerodynamic models for Darrieus-type straight-bladed vertical axis wind turbines. *Renew Sustain Energy Rev*, 12(4), 87–109. https://doi.org/10.1016/j.rser.2006.10.023

7 Gupta, A., Abderrahmane, H., Janajreh, I. (2024). Flow analysis and sensitivity study of vertical-axis wind turbine under variable pitching. *Appl Energy*, 358, 122648. https://doi.org/10.1016/j.apenergy.2024.122648

8 McKenna, R., Leye, P., Fichtner, W. (2016). Key challenges and prospects for large wind turbines. *Renew Sustain Energy Rev*, 53, 1212–1221. https://doi.org/10.1016/j.rser.2015.09.080

9 Jin, X., Zhao, G., Gao, K. (2015). Darrieus vertical axis wind turbine: basic research methods. *Renewable and Sustainable Energy Reviews*, 21(4(41)), 212-225 https://doi.org/10.1016/j.rser.2014.10.021

10 Rakesh, K., Kaamran, R., Alan, S. (2018). A critical review of vertical axis wind turbines for urban applications, *Renew. Sustain. Energy Rev*., 14(8(89), 281–291. https://doi.org/10.1016/j.rser.2018.03.033

11 Sebastian, B., Rosario L., Michele, M. (2014). Design of a vertical-axis wind turbine: how the aspect ratio affects the turbine's performance. *Int. J. Energy Environ. Eng.*, 11(4(37), 333–340. http://dx.doi.org/10.1007/s40095-014-0129-x

12 Wang, Q., Chen, J., Pang, X., Li, S., Guo, X. (2013). A new direct design method for the medium thickness wind turbine airfoil. *Journal of Fluids and Structures*, 19(3(37), 287–301. http://dx.doi.org/10.1016/j.jfluidstructs.2013.08.003

13 Mazarbhuiya, H., Biswas, A., Sharma, K. (2020). Low wind speed aerodynamics of asymmetric blade H-darrieus wind turbine-its desired blade pitch for performance improvement in the built environment, *Braz. Soc. Mech. Sci. Eng*., 42, 326, http://dx.doi.org/10.1007/s40430-020-02408-0.

14 Mohamed, M.H. (2012). Performance investigation of H-rotor Darrieus turbine with new airfoil shapes. *Energy* 47 (1), 522–530. https://doi.org/10.1016/j. energy.2012.08.044.

15 Baizhuma, Z., Kalassov, N., Manatbayev, R., Isataev, M., Seydulla. Z., Georgiev, A. (2026). Time- resolved CFD analysis of torque generation in an L-shaped vertical-axis wind turbine. *Energy*, 344. https://doi.org/10.1016/j.energy.2026.140149

16 Tanasheva, N., Sakipova, S., Minkov, L., Bakhtybekova, A., Shuyushbaeva, N., & Burkov, M. (2021). Study of aerodynamic characteristics of a cylindrical blade with deflector. *Eurasian phys. tech. j.*, 18(3(37), 48–52. https://doi.org/10.31489/2021No3/48-52

17 Tleubergenova, A., Dyusembayeva, A., Tanasheva, N., Bakhtybekova, A., Kutumova, Z., & Mukhamedrakhim, A. (2024). Experimental studies of the performance efficiency of a wind turbine with combined blades. *Eurasian phys. tech. j.*, 21(2(48), 31–37. https://doi.org/10.31489/2024No2/31-37

18 Shaimerdenova, K., Tleubergenova, A., Tanasheva, N., Dyusembaeva, A., Minkov, L., & Bakhtybekova, A. (2025). Aerodynamic improvement of a two-blade magnus wind turbine: numerical and experimental analysis of aerodynamics and pressure distribution. *Eurasian phys. tech. j.*, 22(2 (52)), 79–87. https://doi.org/10.31489/2025N2/79-87.

19 Kalassov, N., Baizhuma, Z., Manatbayev, R., Yershina, A., Isataev, M., Kalassova, A., Seidulla, Z., Bektibay, B., Amir, B. (2025). Integrated approach to aerodynamic optimization of darrieus wind turbine based on the taguchi method and computational fluid dynamics. *Applied Sciences*, 15(10), 5739. https://doi.org/10.3390/app15105739

20 Isataev, M., Manatbayev, R., Seydulla, Z., Bektibai, B., & Kalassov, N. (2024). Study of aerodynamic characteristics of asymmetrical blades and a wind-driven power plant with a vertical axis of rotation. *Applied Sciences*, 14(24), 11654. https://doi.org/10.3390/app142411654

21 Seydulla, Z., Kalassov, N., Isataev, M., Baizhuma, Z., Baizhumanov, K., Kuykabayeva, A., Gabitova, Z., & Satkynova, A. (2026). Performance enhancement of darrieus vawt using modified asymmetric blades: experimental and cfd validation. *Energies*, 19(3), 743. https://doi.org/10.3390/en19030743

22 Isataev, M., Manatbayev, R., Seydulla, Z., Kalassov, N., Yershina, A., & Baizhuma, Z. (2025). Experimental and computational study of the aerodynamic characteristics of a darrieus rotor with asymmetrical blades to increase turbine efficiency under low wind velocity conditions. *Applied System Innovation*, 8(2), 49. https://doi.org/10.3390/asi8020049

23 Baizhuma, Z., Kalassov, N., Isataev, M., Gabitova, Z., Baizhumanov, K., Kuykabaeva, A., Seydulla, Z., Auyezkhan, N. (2026). Investigation of the aerodynamic characteristics in twin-rotor carousel wind turbines. *Energy*, 351, 140833, https://doi.org/10.1016/j.energy.2026.140833

24 Baizhuma, Z., Kalassov, N., Manatbayev, R.K., Isataev, M., Seydulla, Z., Georgiev, A. (2026). Time-resolved CFD analysis of torque generation in an L-shaped vertical-axis wind turbine. *Energy*, 344, 140149. https://doi.org/10.1016/j.energy.2026.140149

25 Kjellin, J., Bülow, F., Eriksson, S., Deglaire, P., Leijon, M., Bernhoff, H. (2011). Power coefficient measurement on a 12 kW straight bladed vertical axis wind turbine. *Renew Energy*, 36, 11, 3050–3053. https://doi.org/10.1016/j.renene.2011.03.031

AUTHORS' INFORMATION

Manatbayev, Rustem – Associate Professor, Al-Farabi Kazakh National University, Department of Thermophysics and Technical Physics, Faculty of Physics and Technology, Almaty, Scopus ID: 55848346700, https://orcid.org/0000-0003-2151-2606, rustemmanatbayev@gmail.com

Kalassov, Nurdaulet – PhD, Al-Farabi Kazakh National University, Department of Thermophysics and Technical Physics, Faculty of Physics and Technology, Almaty, Scopus Author ID: 57222177960, https://orcid.org/0000-0003-3709-5544, kalasov.nurdaulet@gmail.com

Seydulla, Zhanibek – PhD, Al-Farabi Kazakh National University, Department of Thermophysics and Technical Physics, Faculty of Physics and Technology, Almaty, Scopus Author ID: 57202515147, https://orcid.org/0000-0003-0413-6557, seidulla.zhanibek@kaznu.edu.kz

Isataev, Muhtar – Candidate of Physical and Mathematical Sciences, Al-Farabi Kazakh National University, Department of Thermophysics and Technical Physics, Faculty of Physics and Technology, Almaty, Scopus ID: 56943370900, https://orcid.org/0000-0001-8248-670X , muhtar.isataev@kaznu.kz

Baizhuma, Zhandos – PhD, Al-Farabi Kazakh National University, Department of Thermophysics and Technical Physics, Faculty of Physics and Technology, Almaty, Scopus Author ID: 57205433240, https://orcid.org/0000-0002-1226-7736, zhandos.baizhuma@kaznu.kz

Kuykabayeva, Aizhan – PhD, Al-Farabi Kazakh National University, Department of Thermophysics and Technical Physics, Faculty of Physics and Technology, Almaty, Scopus Author ID: 34968215400, https://orcid.org/0000-0002-0905-4422, a.kuikabaeva1@gmail.com

Kozhash, Rasul – Bachelor's student, Al-Farabi Kazakh National University, Department of Thermophysics and Technical Physics, Faculty of Physics and Technology, Almaty, https://orcid.org/0009-0005-3583-0850 , kozhash@list.ru